Design, Aerodynamic Calculation and Manufacturing using CFRP and Additive Manufacturing of a small Tilt-Rotor UAV for Railway Inspection

Raluca MAIER[1], Andrei MANDOC*,[1], Stefan GHERASIM[1],
Stefan PETCULESCU[1], David MANOLACHE[2], Razvan CARLANESCU[1]

*Corresponding author
[1]Composite Materials Department, National Research and Development Institute for Gas Turbines INCDT COMOTI,
220 D Iuliu Maniu Av., Bucharest, 061126, Romania,
raluca.maier@comoti.ro, andrei.mandoc@comoti.ro*, stefan.gherasim@comoti.ro, stefan.petculescu@comoti.ro, razvan.carlanescu@comoti.ro
[2]Thales Systems Romania,
319 G Splaiul Independentei Av., Bucharest, 60043, Romania,
david.manolache@thalesgroup.com

DOI: 10.13111/2066-8201.2020.12.4.10

Received: 13 July 2020/ Accepted: 21 October 2020/ Published: December 2020

Abstract: *The present paper aims to develop a small scale Unmanned Aerial Vehicle for railway inspection. The development process and structure manufacturing aimed at a low complexity technological process both to meet market requirements and to be economically efficient. To define the architectural structure and its components in the design process, a NACA 0024 aerodynamic profile was selected out of two proposed airfoils. The novelty of this concept is the double benefit of the wing, which serves as a cargo bay while uses a low-cost manufacturing technology, incorporating the 3D printing process. Further, a simplified preliminary aerodynamic calculation was performed, the model was manufactured using composite materials reinforced with carbon fibre while other key components have been obtained using the 3D printing technology. In the end, the manufacturing process was a success and the unmanned aerial vehicle was designed and manufactured specifically that its flight envelope meets the requirements of the mission.*

Key Words: *unmanned aerial vehicle, manufacturing, carbon fibre composite, 3D printing, additive manufacturing*

1. INTRODUCTION

The proposed project is looking to fabricate a wing structure with vertical take-off and landing (VTOL), which will serve as an unmanned aircraft vehicle to observe and report possible damage of the railroads. Thus, in order to achieve the objective, a detailed research on other types of VTOL Unmanned Aerial Vehicle (UAV) is made and there are two important types: Flying wing UAVs and Tilt-rotors UAVs [1-3]. The UAVs presented above have both advantages and disadvantages when compared. One of the general problems is manifested in the stage of transition from VTOL to horizontal flight and is represented by the tilting rotors

or wings. Failure may occur in the joint area or instability may be induced in the transition between flights types (2nd) [4]. A major disadvantage for the first case presented would be that, during the flight transition, instability can occur and requires good coordination between the remote pilot and the UAV [5].

2. EXPERIMENTAL PART. SIMPLIFIED PRELIMINARY AERODYNAMIC CALCULATION AND ANALYSIS OF AERODYNAMIC PROFILES

Before the design phase, multiple steps were necessary to determine the optimal airfoil of the wing geometry. Two airfoils which can be found in Figure 1 were selected to be evaluated with an open source software called XFLR 5 in order to select the best option.

Because it is desired to place the electrical components of the drone inside the wing, it was necessary to use an airfoil with maximum thickness of 6 cm at the root chord and 4 cm at the tip of the wing. Hence, modifications of the airfoils were required to meet the demands above, although maintaining the position of the maximum thickness at a maximum of 27% of the chord was taken into account due to a thorough research on specialty papers, which followed the effects that the maximum thickness and its position can have over the gliding ratio or the power factor [4].

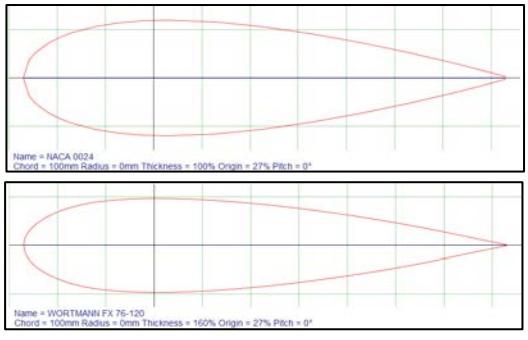

Fig. 1 – a). NACA 0024 and b) FX 76 airfoils

To improve the manufacturing time, a symmetric airfoil was imposed. In Figures 2, 3 the charts from the analysis of the two airfoils were plotted, NACA 0024 in gray and FX 76 in blue. The polar data obtained were exported in an EXCEL document, which was used, together with the formula, to calculate the power factor and their gliding ratio.

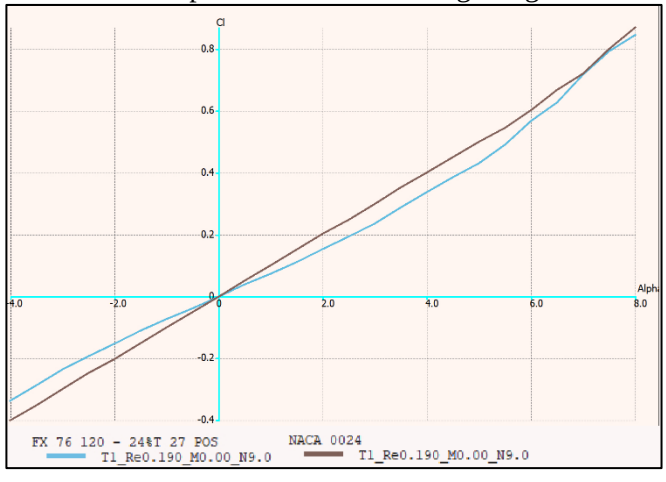

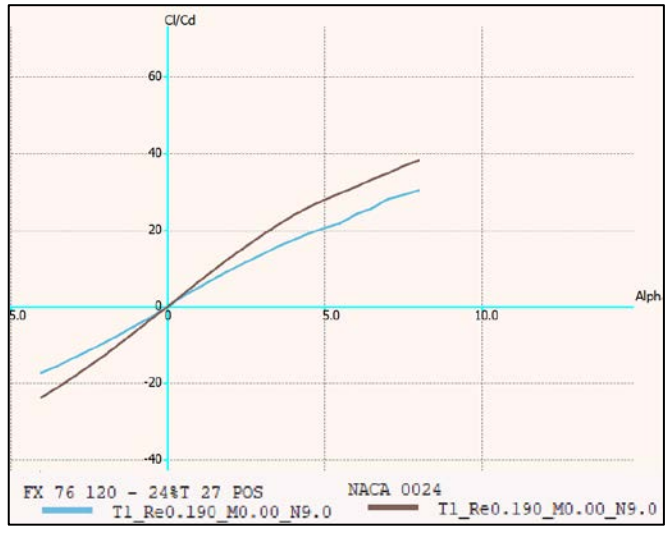

b

Fig. 2 – a) Lift coefficient based on the angle of the leading edge; b) The ratio between the lift coefficient and drag coefficient based on the angle of the leading edge

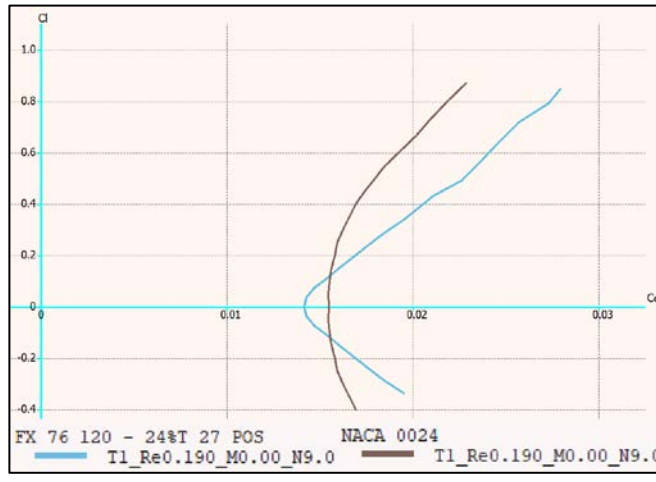

a

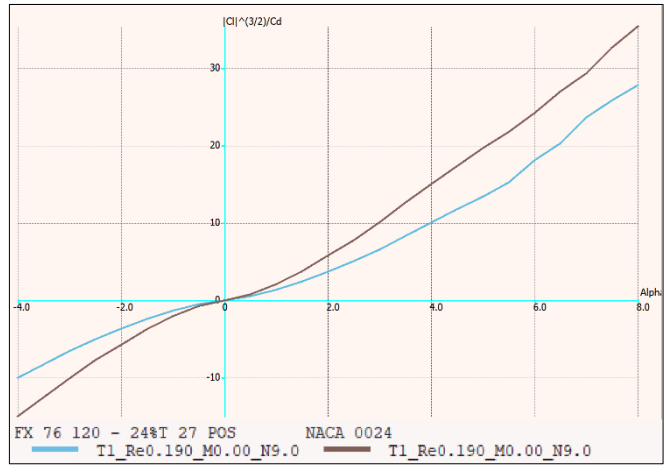

b

Fig. 3 – a) Lift coefficient based on the drag coefficient; b) Power factor based in the angle of the leading edge

The analysis of the airfoils was made for a Re (Reynolds number) of 190000, at angles of the leading edge ranging between -4 and 8 degrees. Based on the analysis of the two airfoils performances it was found that NACA 0024 airfoil reacts the best when compared to XF76 airfoil, in terms of aerodynamic efficiency given by minimum and maximum power factor and gliding ratio, as seen in Table 1.

Table 1. – The characteristics of the selected airfoils

1	NACA 0024	Minimal power factor – 0.73 Maximum power factor – 35.42 Minimal gliding ratio – 3.27 Maximum gliding ratio – 38.01
2	XF 76	Minimal power factor – 0.52 Maximum power factor – 27.83 Minimal gliding ratio – 2.67 Maximum gliding ratio – 30.27

3. GEOMETRY OF THE WING

After choosing the NACA 0024 airfoil, the next step was to establish the wing geometry considering the restrictions imposed by the contractor.

Table 2. – Input atmospheric data

$\rho_0 = 1.225[\frac{kg}{m^3}]$	Standard density of air
$T_0 = 288.15[K]$	Standard temperature
$H = 100[m]$	Maximum height of flight
$g = 9.81[\frac{m}{s^2}]$	Gravitational acceleration
$v_{inf} = 15[\frac{m}{s}]$	Velocity of air
$\nu = 15.68 \cdot 10^{-6}$	Kinematic viscosity (at $T = 300K$)

From the data in Table 2 we can obtain the following information:

$$T = T_0 - 0.0065 \cdot H = 287.5[K] \quad Temperature \tag{1}$$

$$\rho = \rho_0 \cdot (1 - 0.0000226 \cdot H)^{4.225} = 1.213\left[\frac{kg}{m^3}\right] \quad Air\ Density \tag{2}$$

$$a = 20.0519 \cdot \sqrt{T} = 339.997\left[\frac{m}{s}\right] \quad Speed\ of\ sound \tag{3}$$

$$M = \frac{v_{inf}}{a} = 0.035 \quad Mach\ number \tag{4}$$

For the wing geometry, the wing span $b_A = 1[m]$, root chord $c_0 = 0.25[m]$ and tip chord $c_e = 0.18[m]$. These data were provided for the following calculations:

$$tr1 = \frac{b_A}{2} = \frac{2}{2} = 0.5 \quad Half\ wing\ span \tag{5}$$

$$S_A = (c_0 + c_e) \cdot tr1 = 0.215[m^2] \quad Wing\ surface \tag{6}$$

$$S_{wet} = S_A \cdot 2.036 = 0.438[m^2] \quad Wet\ surface\ of\ the\ wing \tag{7}$$

$$cmg = \frac{S_A}{b_A} = 0.215[m] \quad Geometric\ mean\ chord \tag{8}$$

The chord function along the wing span results from the following:

$$c_A(y) = \frac{c_e - c_0}{tr1} \cdot (y) + c_0 \tag{9}$$

$$c_A = \left(\frac{b_A}{2}\right) = 0.1 \tag{10}$$

The ratio between the wing span and the mean chord line can be determined as such:

$$\lambda_A = \frac{b_A^2}{S_A} = 4.651 \tag{11}$$

The mean aerodynamic chord was obtained with the following formula:

$$cma_A = 2 \cdot \frac{\int_0^{\frac{b_A}{2}} c_A(y)^2 dy}{S_A} = 0.217 \tag{12}$$

The trapezoidal ratio of the wing was calculated as such:

$$\tau = \frac{c_0}{c_e} = 1.389 \tag{13}$$

4. THE ANALYSIS OF THE TRANSITION SPEED

In order to make an analysis of the minimal horizontal speed necessary for the drone to make the complete transition to horizontal flight, the following parameters must be defined:

$$m_e = 1.9[kg] \quad Electronics\ weight \tag{14}$$

$$m_a = 1.297[kg] \quad Wing\ weight \tag{15}$$

From these data we could determine:

$$m_{tot} = m_a + m_e = 3.198[kg] \quad Total\ mass\ (with\ load) \tag{16}$$

$$G_{tot} = m_{tot} \cdot g = 31.363[kg \cdot \left(\frac{m}{s^2}\right)] \quad Total\ weight \tag{17}$$

Furthermore, the angle of the leading edge was selected to be optimal for flight and the lift and drag coefficients were extracted:

$$C_{LW} = C_{L1}(\alpha) = 0.72 \tag{18}$$

$$C_{DW} = C_{D1}(\alpha) = 0.021 \tag{19}$$

Considering this input data, one can calculate the optimum speed for transition to horizontal flight:

$$V_T = \sqrt{\frac{2 \cdot G_{tot}}{\rho \cdot S_A \cdot C_{Lmax}}} = 18.272 \quad Minimal\ transition\ speed\ [m/s] \tag{20}$$

$$V_D = 1.1 \cdot V_T = 20.1 \quad 10\% \; over \; minimal \; transition \; speed(optimal) \; [m/s] \tag{21}$$

To graphically represent the the available and required thrust, a known model of electric motor was chosen (AXI Golden 2826/10) and with the help of a software available online [6] the necessary data for plotting the graph in Fig. 4 were obtained.

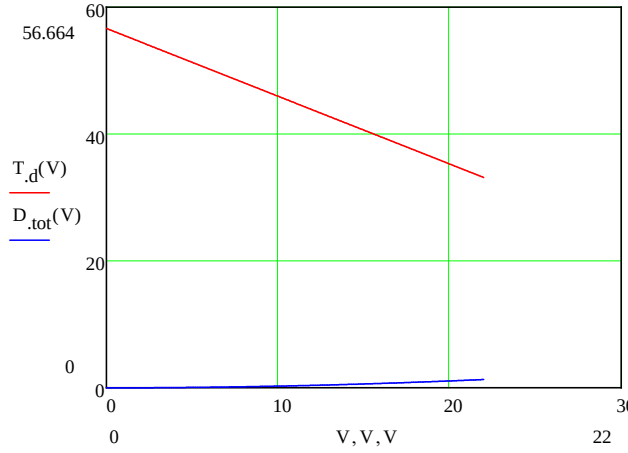

Fig. 4 – The available (T.d) and required (D.tot) thrust based on velocity

5. AERODYNAMIC ANALYSIS OF THE WING

Once these data were obtained, the next step was the aerodynamic analysis of the wing in XFLR5. The wing was analysed at a cruising speed of 12 m/s, having a total mass of 3.198 kg. Firstly, downwash was analysed in Figure 5(a). The result shows variations between the root chord and the tip of the wing. The fact that in the central area of the wing, the downwash maintains its intensity at a steady level, indicates good stability and a constant lift coefficient.

These variations that appear at the tips of the wings can be minimized by increasing the aspect of the wing or by modifying the tips of the wings with a twist angle.

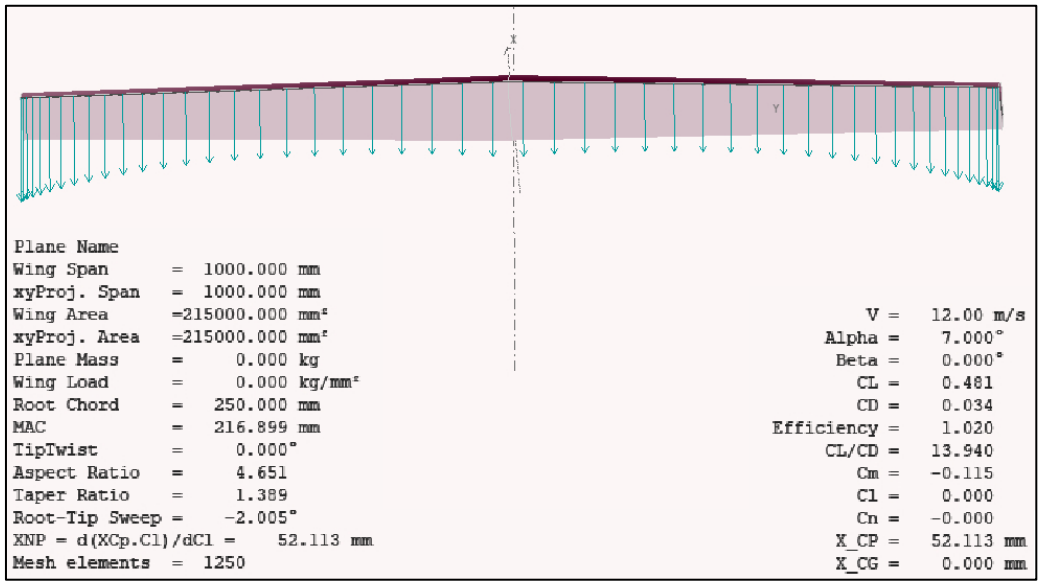

a

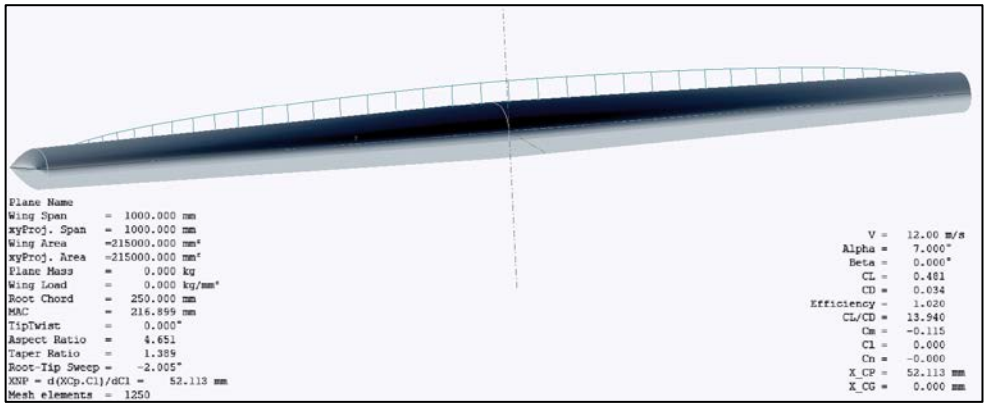

b

Fig. 5 – a) Downwash; b) Distribution of lift coefficient

In Figures 5(b) and 6(a) we can observe the distribution of the lift coefficient along the wing. It has an average of 0.5 maintaining itself high in the central part of the wing and decreasing to 0 to the tips of the wings, indicating a normal behaviour for a well-defined wing.

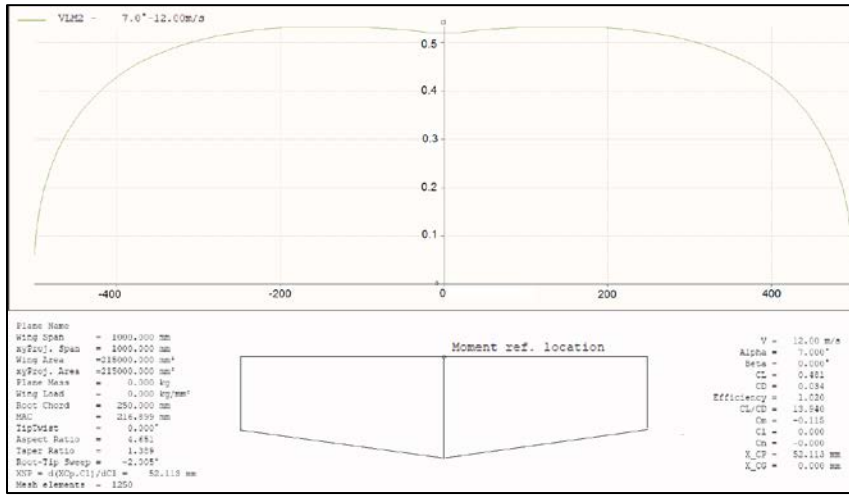

a

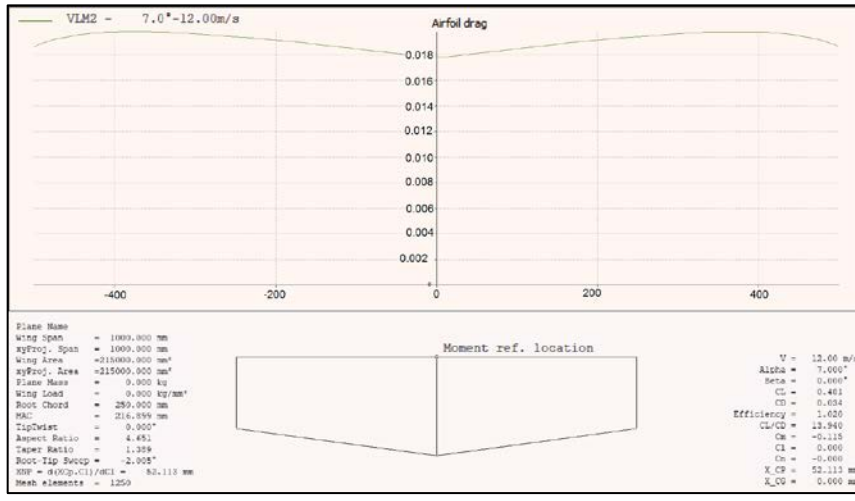

b

Fig. 6 – a) The distribution of lift coefficient on the wing span; b) Geometric distribution of the drag coefficient

Another aspect which needs increased attention because of the modification in maximum thickness of the airfoil but also, often met in symmetrical airfoils, is the distribution of the drag coefficient. As it can be observed in Figure 6(b), the distribution of the drag coefficient rises at the tips of the wings and drops towards the center/centre, behaviour which should be different considering the Reynolds number in Figure 7(a).

According to Figure 7(a), the distribution of the drag coefficient should fall along the wing span. This phenomenon is due to the vortices that appear at the wing tips and can be observed in Figure 7(b). The phenomenon is considered, in this case, a controlled one because of the indicator of efficiency shown by the simulation which is calculated depending on the lift and drag coefficient. This indicates an efficiency of 100%.

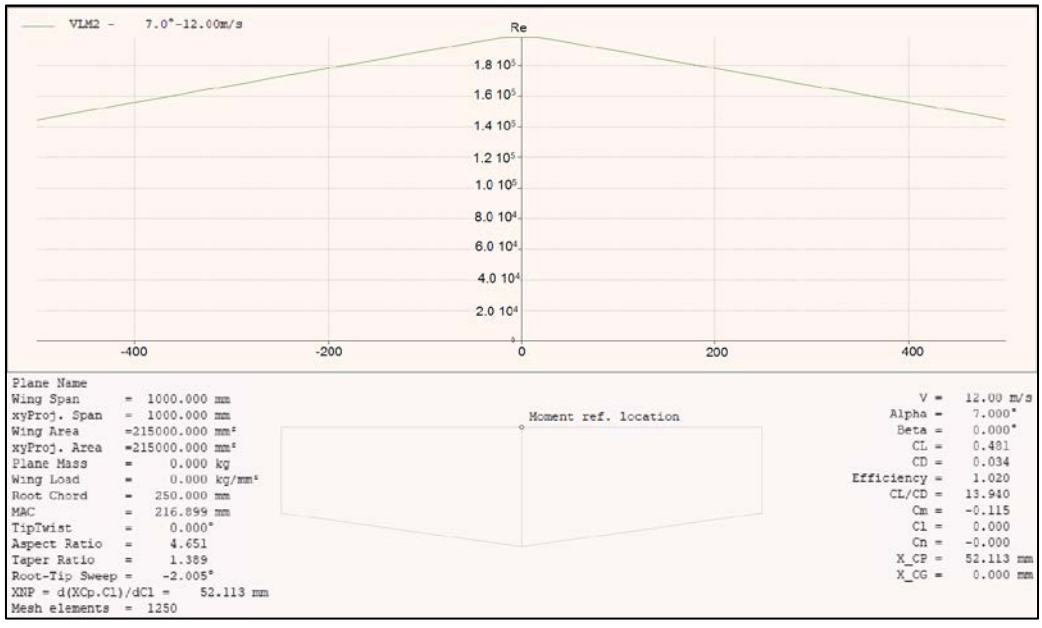

a

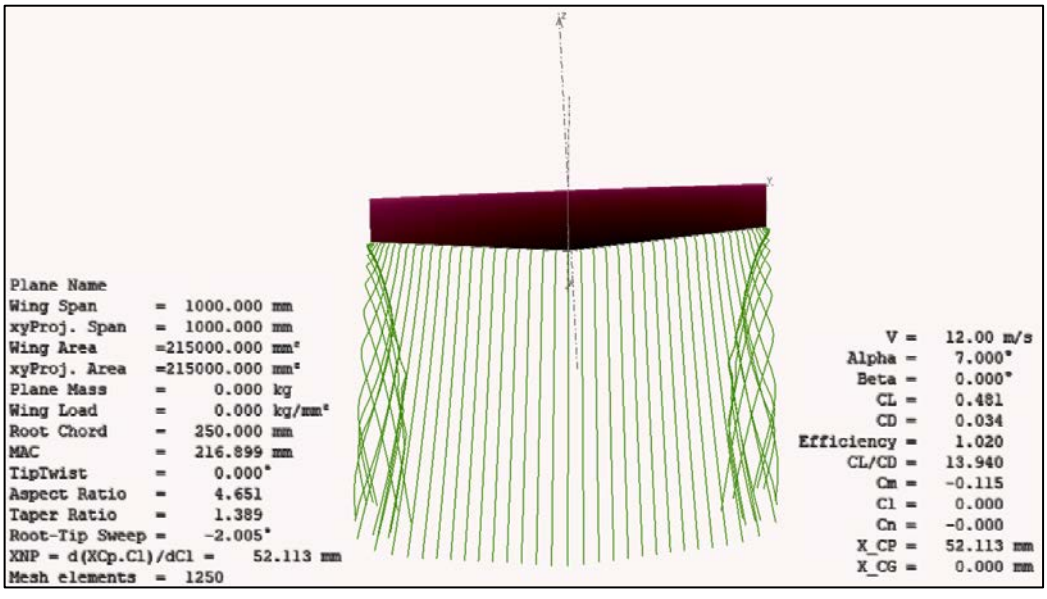

b

Fig. 7 – a) Geometrical distribution of Reynolds number; b) Vortices generated at the wing tips

The efficiency of the wing is indicated by an elliptical shape of the distribution of the lift coefficient which can be observed in Figure 6(a).

For a future optimization of the aerodynamics of the wing which can lead to a reduction of vortices created at the wing tips, three variants can be proposed: change of wing geometry at wing tips, use of another airfoil in combination with NACA 0024, on a defined section of the wing which includes the tips of it and usage of winglets at the wing tips.

6. DESIGN OF THE WING AND SUBASSEMBLIES

To conclude the previous steps and proceed to the manufacturing part, this section follows the design of the airfoil, structure and 3D printed joints. Using the analysis of the profile, the structures of the wing and the airfoil were defined using imported coordinates points of NACA0024 profile from XFLR5 and Solid Edge as a base for CAD part.

Starting from the airfoil, the reinforcement elements that are present at the ends and center of the wing were designed (Fig. 8). They can also be seen as part of the assembly in Fig. 10.

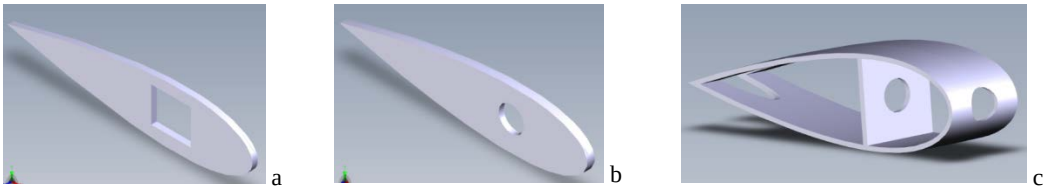

Fig. 8 – a) Exterior reinforcement profile; b) Interior reinforcement profile; c) Center reinforcement

To use the VTOL maneuver, it was necessary to create a joint mechanism with an integrated motor support. Two of the electric motors are mounted on the exterior part of the wing, being responsible with providing the VTOL and traction capabilities (Fig. 9).

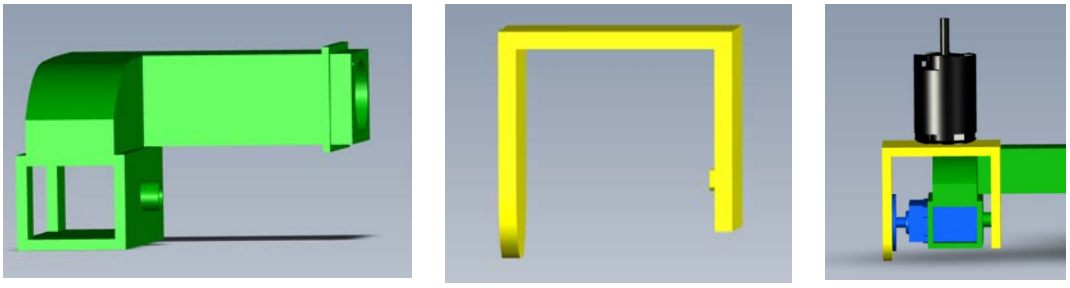

Fig. 9 – a) Arm for servo and joint; b) Electrical engine support; c) Assembled joint

The other two electrical motors, designed to maintain the alttitude are mounted in front and rear of the wing, respectively, on a carbon fiber tube. For mounting the motors on the carbon tubes, two symmetrical elements have been designed to meet this requirement.

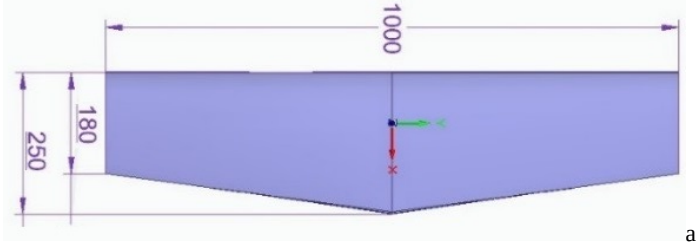

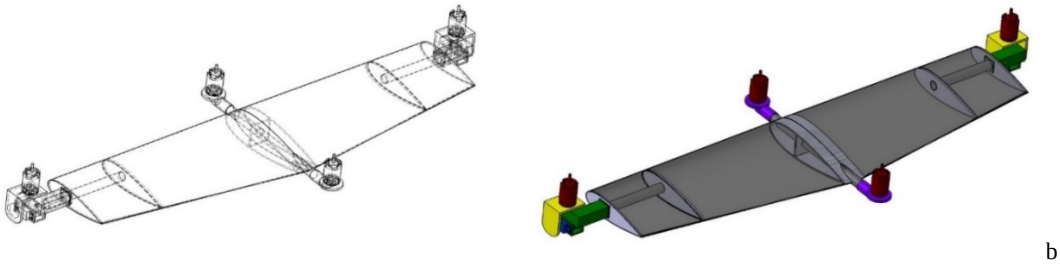

b

Fig. 10 – a) Dimensions and b) final assembly drawings in Solid Edge

7. MANUFACTURING PART

The building of the UAV was posible with 3D printing technology and composite materials. The printed parts were composed of UV curing resin, using a Formlab 2 printer. The CAD parts were introduced into the printer software, where the amount of resin needed for each part was calculated. After printing, another UV curing cicle was required for 3 to 4 hours, then the parts were cleaned using acetone. Their final form can be seen in Figure 11(a).

a b c

Fig. 11 – a) 3D printed parts using UV curing resin; b) Wing from extruded polystyrene cutted with hot wire; c) Access points for electronics

Starting from the CAD drawings, it was possible to create the wing from extruded polystyrene cutted with hot wire (Fig. 11(b)) used as a mould for the carbon fiber composite laminate wing shells. The skins/shells were manufactured from 4 layers of carbon fiber Twill2×2/ 200g/m^2 impregnated with epoxy resin RESOLTECH 1050/1059. The mould was covered with release film (Fig. 11(b)) in order to facilitate the extraction of the carbon fiber wing skins, followed by the hand-layup of the fibers. On top of the last layer, a PVC film was

placed in order to obtain a smooth surface of the skins, for aerodynamic purposes. Another layer of release film was placed on top of the PVC film in order to keep the vacuum bag from coming into direct contact with the resin. The whole assembly was then introduced inside a vacuum bag and the vacuum process started for a period of 24H following a post curing process of 15 hours at 60^{o}C.

After the upper and lower skin/shell were obtained, the first step was to cut the desired acces points for the electronics, as seen in Figure 11 (c). Later on, a hinge was added together with the lids and a servo-mechanism was mounted to close and open it as desired (Figure 13(b)). The reinforcement elements were fitted on one of the shells with an elastomer based ballistic adhesive while the carbon tubes were cut at the appropiate dimensions and fitted through the special holes present in the reinforcement structures, as seen in Figure 12(a) and 11(a). Two tubes were fixed with the elastomer based ballistic adhesive at both end of the wings. Another two tubes were fitted through the same technological process at the root chord. Their roles were to offer structural resistance and as a base for mounting the motor supports that were 3D printed. After leaving the adhesive cure for 24H, the second skin was added to close the wing. The same adhesive was used at every contact point between the reinforcement structures and the skin, as well as along the leading and trailing edge (Figure 12(b, c)).

Fig. 12 – Three stages of the manufacturing process from left to right

The final steps were adding three landing supports and the camera required for the mission. The camera was fitted using small screws from the inside of the wing and with double adhesive band. The final stage of the UAV can be seen in Fig. 13 a).

a

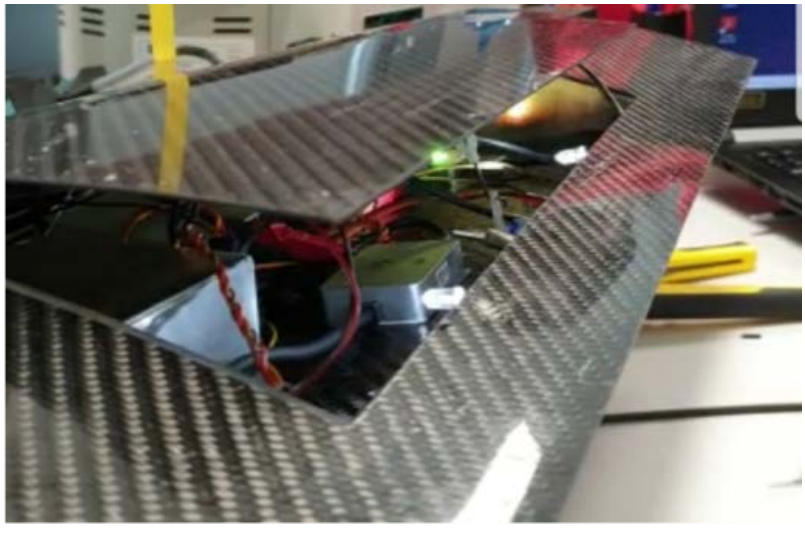

b

Fig. 13 – a) Final form of the UAV; b) Electronics hatch

8. MANUFACTURING SPECIFICATIONS

For the 3D printing processes, a Form 2 printer was utilised from formlabs. Two types of UV cured resin were taken into consideration, Clear Resin and Rigid Resin which were subjected to post-curing processes using an oven and UV light.

Due to several cracks that started to appear on the parts printed using Clear Resin during their processing (inserting carbon fibre tubes, drilling, etc.), the parts were re-printed using a more resistant resin (Rigid Resin).

Also, a higher temperature resistance was required given the necessity of a post-curing process of the elastomer adhesives that was to be used for the joint sections. Their specifications can be checked in Table 3.

The rigid resin had a better behaviour when subjected to post-processing activities such as drilling and inserting the carbon fibre tubes.

Table 3. – Properties of the printing materials

Material Properties	Rigid Resin	Standard/Clear Resin
Ultimate Tensile Strength	75 MPa	65 MPa
Tensile Modulus	4.1 GPa	2.8 GPa
Elongation at Break	5.6%	6%
Flexural Stress at 5% Strain	121 MPa	-
Flexural Modulus	3.7 GPa	2.2 GPa
Notched IZOD	18.8 J/m	25 J/m
Heat Deflection Temp at 1.8 MPa	74ºC	58.4ºC

The mould of the wing was manufactured from hot-wired cut polystyrene. A metal wire was fixed and tensioned while heated using an electrical resistance at about 200ºC. The polystyrene block was cut exactly to the span of the wing and two pieces of plywood, shaped according to the wing airfoil, were glued to each side to serve as guidance for the hot wire. Extruded polystyrene was used, due to prior experience, given its better resistance and higher surface quality after the hot wire cutting process.

The wing skins were manufactured using four, 0.3mm thickness layers of carbon fiber Twill2x2/ 200g/m^2 impregnated by hand-layup with epoxy resin RESOLTECH 1050/1059 of 1.12g/cm^3 density. The stacking sequence was [0º -45º +45º 0º]. The carbon fibre characteristics are presented in Table 4 and the resin characteristics are shown in Figure 14.

Table 4. – Properties of carbon fibre

Material Characteristics	Carbon Fibre
TRACTION	
Tensile strength	1 302 MPa
Tensile Modulus	95 GPa
Tensile strain	1%
FLEXION	
Flexural Strength	1 250 MPa
Flexural Modulus	87 GPa

Values on non reinforced resin after 24h at 23°C + 15h at 60°C

	1050/1059
TRACTION (ISO 527-2)	
Modulus (MPa)	3321
Max stress(MPa)	77,5
Failure stress (MPa)	74,5
Failure strain (%)	3,7
FLEXION (ISO 178)	
Modulus (MPa)	3390
Max stress(MPa)	125,1
Failure stress (MPa)	116.9
Failure strain (%)	6,3
COMPRESSION (ISO 604)	
Modulus (MPa)	2147
Failure stress (MPa)	86

Fig. 14 – RESOLTECH 1050/1059 resin properties

In the polymerization process, the following auxiliary materials were used: release agent (preventing the resin to bond with the mould and other parts used during the process that are not to be part of the obtained laminate), bleeder fabric (contains the excess resin), release film (prevents the resin to pass to other auxiliary materials during the polymerization process), breather (facilitates the uniform vacuum bagging on the entire surface of the laminate), vacuum bag and mastic tape sealant. All the auxiliary materials are aerospace graded and were acquisitioned from AIRTECH EUROPE SARL.

An elastomeric adhesive, ADEKIT A 252, was used for all the joints, as presented in chapter 7. A curing process of 16 hours at 70°C was needed in order to obtain the properties presented in Figure 15.

Tensile strength, MPa	7	ISO 37
Elongation at break, %	300	
Young Modulus, MPa	8	
Recommended application temperature, °C	15 - 25	-
Working temperature, °C	-40 to 120	LT-006-B

Fig. 15 – Adekit A 252 properties

The carbon tubes used were acquisitioned from SIERRA MODELLSPORT and were manufactured using the roll-wrap technology. The tubes had an internal diameter of 18mm and an external diameter of 20mm. They were used for both structural purposes and for guiding and protecting the wires connecting the electric motor and tilt mechanism servos to the receiver.

All other elements of the manufacturing process (PVC film, hinges, etc.) are not discussed as they can be found in any available hardware store.

9. CONCLUSIONS

The architectural structure and the drone components have been defined. The simplified preliminary aerodynamic calculus was conducted in order to find the right configuration to start the manufacturing processes, using composite materials reinforced with carbon fiber.

The UAV was specially designed so that its flight envelope meets the requirements of the mission. In this manner, an aerodynamic profile was down selected and the input parameters were thoroughly analysed (maximum altitude, transition velocity, cruise speed, needed thrust, battery capacity) in order to achieve a minimum of 20 minutes of flight. Furthermore, to enhance the visual inspection quality, it was necessary that the UAV could operate at lower cruise speed and altitude. For peak performance an optimum of 12m/s cruise speed and a height of flight of 100m were calculated. A preliminary design was obtained and following the XFLR5 software aerodynamic analysis it was concluded that it matches the desired flight envelope.

Using 3D printing technology, the reinforcement components have been made, together with the supports for the integration of the motors and other specific elements. The development and the manufacturing process of the structure aims at defining a technological process with minor complexity, which could meet the requirements of the beneficiary being at the same time economically efficient.

ACKNOWLEDGMENTS

The work was founded under the Economic contract 48P within Romanian Research Institute for Gas Turbines COMOTI with the title "Design, simplified preliminary aerodynamic calculation and structure fabrication of an Unmanned Aircraft Vehicle".

REFERENCES

[1] A. S. Saeed & A. B. Younes & C. Cai & G. Cai, A survey of hybrid Unmanned Aerial Vehicles, *Progress in Aerospace Sciences*, 10.1016/j.paerosci.2018.03.007, 2018.

[2] Y. Zhou, H. Zhao and Y. Liu, An evaluative review of the VTOL technologies for unmanned and manned aerial vehicles, *Computer Communications*, doi: https://doi.org/10.1016/j.comcom.2019.10.016, 2019.

[3] S. Gupta & M. Ghonge & P. Jawandhiya, Review of Unmanned Aircraft System (UAS), *International Journal of Advanced Research in Computer Engineering & Technology*, **9**, 10.2139/ssrn.3451039, 2013.

[4] A. M. Kamal, A. Ramirez-Serrano, Design methodology for hybrid (VTOL + Fixed Wing) unmanned aerial vehicles, *Aeronautics and Aerospace Open Access Journal***,** Volume **3**, Issue 3, 2018.

[5] T. Matsumoto & K. Kita & R. Suzuki& A. Oosedo & K. Go & Y. Hoshino & A. Konno & M. Uchiyama, A Hovering Control Strategy for a Tail-Sitter VTOL UAV that Increases Stability against Large Disturbance, *2010 IEEE International Conference on Robotics and Automation*, 2010.

[6] * * * https://www.ecalc.ch/motorcalc.php